3-D synthetic aperture radar surveys

C. Prati, and F. Rocca

ABSTRACT

Usually, only the modulus of the focused image is considered for SAR (Synthetic Aperture Radar) surveys. To get information on the terrain elevation, we compare the phases of picture elements of focused images gathered in multiple satellite passes.

MULTIPLE SAR SURVEYS

System geometry

Let us suppose that the same area of the earth's surface can be observed from two different SAR systems (Synthetic Aperture Radar; Fitch, 1988; Ottolini, 1987; Rocca, 1987) moving along parallel orbits (Zebker et al., 1985). Figure 1 represents this experimental condition. For the sake of simplicity, Figure 2 displays a cross-section of Figure 1 orbits.

Let S_1 and S_2 be the positions of the two satellites; P_1 and P_2 will serve as the positions of two point scatterers on the terrain. The backscattered field of P_1, measured in S_1 with a phase $\phi_{1,1}$, will be measured in S_2 with a different phase, $\phi_{2,1}$, due to the different travel time. The phase difference between measurements in S_1, S_2 is:

$$\psi_1 = \phi_{2,1} - \phi_{1,1} = \frac{2\omega_0}{c}(\overline{S_2P_1} - \overline{S_1P_1}), \tag{1}$$

where ω_0 is the transmitted wave angular frequency and c is the speed of light.

If we consider the point P_2, a different value ψ_2 will result:

$$\psi_2 = \phi_{2,2} - \phi_{1,2} = \frac{2\omega_0}{c}(\overline{S_2P_2} - \overline{S_1P_2}). \tag{2}$$

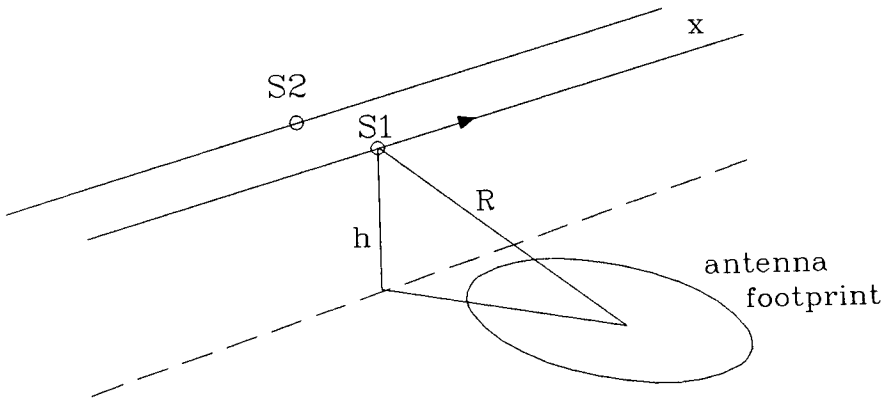

FIG. 1. SAR geometry for multiple satellite passes.

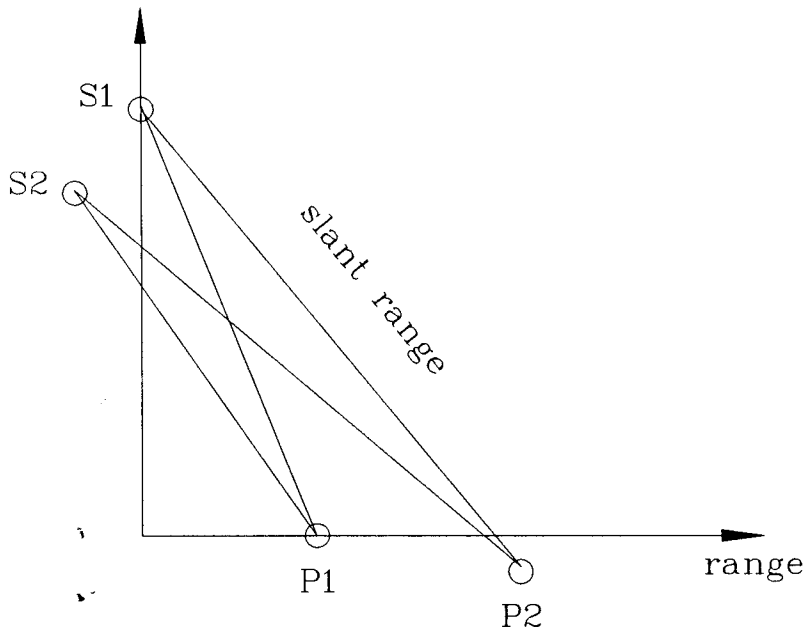

FIG. 2. Cross-section normal to the orbit of Figure 1.

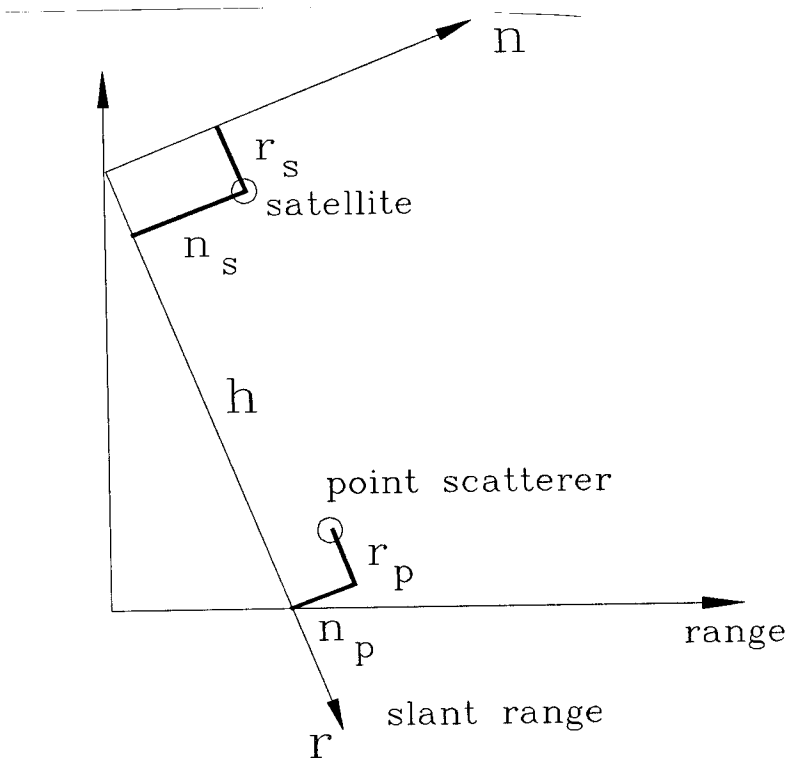

FIG. 3. Cross-section normal to the orbit of Figure 1.

If $F_1(P_i)$ and $F_2(P_i)$ are the complex focused SAR images of the same point P_i as observed by the two satellites S_1 and S_2, respectively, the composite complex image

$$F_3(P_i) = F_1(P_i)F_2^*(P_i) = \mid F_1(P_i) \mid\mid F_2(P_i) \mid e^{j\psi_i} \quad , \tag{3}$$

will have phase

$$\psi_i = \frac{2\omega_0}{c}(\overline{S_2P_i} - \overline{S_1P_i}) \quad . \tag{4}$$

Phase images

Let us now find the expression of $\psi_2 - \psi_1$ as a function of the difference in terrain elevation between P_1 and P_2. Looking at Figure 3, the distance between a point scatterer of coordinates $[(h + r_p), (n_p)]$ and a satellite of coordinates $[(r_s, n_s)]$ is:

$$d = \sqrt{(h + r_p + r_s)^2 + (n_p - n_s)^2} \quad . \tag{5}$$

The phase difference ψ of the backscattered electromagnetic field measured by two satellites respectively positioned in $(0,0)$ and (r_s, n_s), after focusing, can be approximated with the differential:

$$\psi = \frac{\partial \phi(r_p, r_s, n_p, n_s)}{\partial n_s} \mid_{r_s=n_s=0} n_s + \frac{\partial \phi(r_p, r_s, n_p, n_s)}{\partial r_s} \mid_{r_s=n_s=0} r_s. \tag{6}$$

The variation of this function with respect to the backscatterer position can then be expressed as:

$$\Delta\psi = \frac{\partial \psi(r_p, r_s, n_p, n_s)}{\partial n_p} \mid_{r_p=n_p=0} n_p + \frac{\partial \psi(r_p, r_s, n_p, n_s)}{\partial r_p} \mid_{r_p=n_p=0} r_p =$$

$$= \frac{\partial^2 \phi}{\partial n_p \partial n_s} \mid_{r_p=r_s=n_p=n_s=0} n_p n_s + \frac{\partial^2 \phi}{\partial n_p \partial r_s} \mid_{r_p=r_s=n_p=n_s=0} n_p r_s +$$

$$\frac{\partial^2 \phi}{\partial r_p \partial n_s} \mid_{r_p=r_s=n_p=n_s=0} r_p n_s + \frac{\partial^2 \phi}{\partial r_p \partial r_s} \mid_{r_p=r_s=n_p=n_s=0} r_p r_s. \tag{7}$$

It can be shown, however, that all the second derivatives in equation (7) are zero, except for the first one which depends on the point and satellite displacements normal to the slant range direction. The final expression of $\Delta\psi$ is then

$$\Delta\psi = \frac{2\omega_0}{ch} n_s n_p. \tag{8}$$

In the case of flat terrain, equation (8) gives

$$\Delta\psi = \frac{2\omega_0}{ch \tan\alpha} n_s \Delta r, \tag{9}$$

where Δr is the image slant range displacement, and α the off-nadir angle of the SAR antenna. The phase difference $\Delta\psi$ has, thus, a linear dependence upon slant range. Limiting its values to the range $-\pi$ and $+\pi$, we do, however, see a saw-tooth function with a constant period

$$\Delta R = \frac{\pi ch \tan\alpha}{\omega_0 n_s}. \tag{10}$$

Alternatively, if the terrain has a constant slope of θ degrees, and is not flat, as Figure 4 illustrates, the following expression of $\Delta\psi$ holds:

$$\Delta\psi = \frac{2\omega_0}{ch \tan(\alpha - \theta)} n_s \Delta r. \tag{11}$$

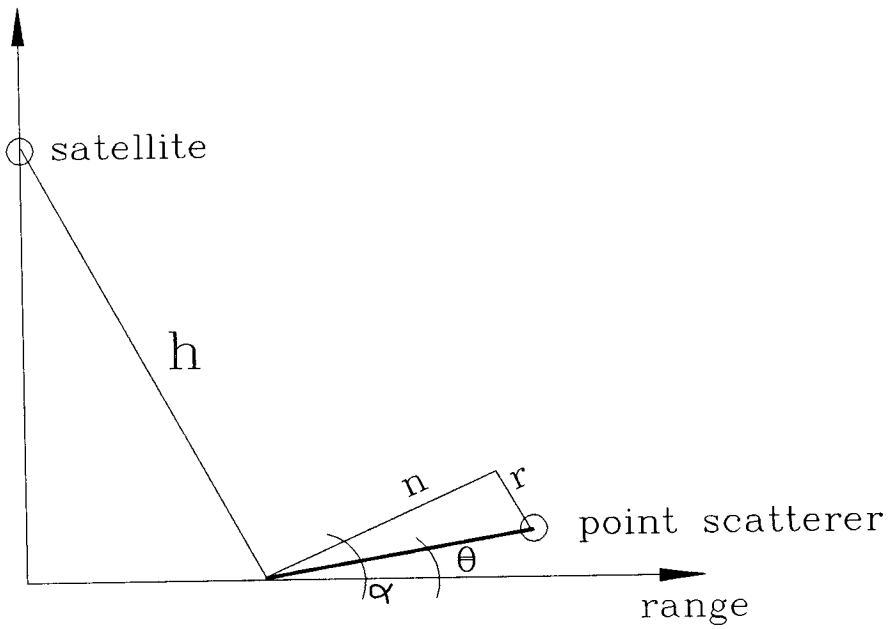

FIG. 4. Effect of terrain elevation upon the computation of $\Delta\psi$

In this case, the phase will be again a saw-tooth function, but with a different period

$$\Delta R = \frac{\pi c h \tan(\alpha - \theta)}{\omega_0 n_s}. \tag{12}$$

The terrain slope can then obviously be measured without ambiguity only within a 90 degrees range between $90-\alpha$ and α. Consequently, an off-nadir angle of $\alpha = 45$ degrees seems to be the most reasonable solution.

Changing the phase wrapping period

We have shown so far that in looking at the phase image of $F_3(P)$ we can find the average slope of the terrain, but not the elevation variance. Consider, for example, the two point scatterers of Figure 5a: they have the same drop with respect to reference level, but their normal displacement n_p is different. As a consequence of equation (9), they do not produce the same phase difference $\Delta\psi$.

It is possible to overcome the problem by modifying the complex image $F_3(P)$; by zeroing the phase difference $\Delta\psi$ relative to the flat terrain by multiplying $F_3(P)$ in the slant range dimension, times the complex exponential

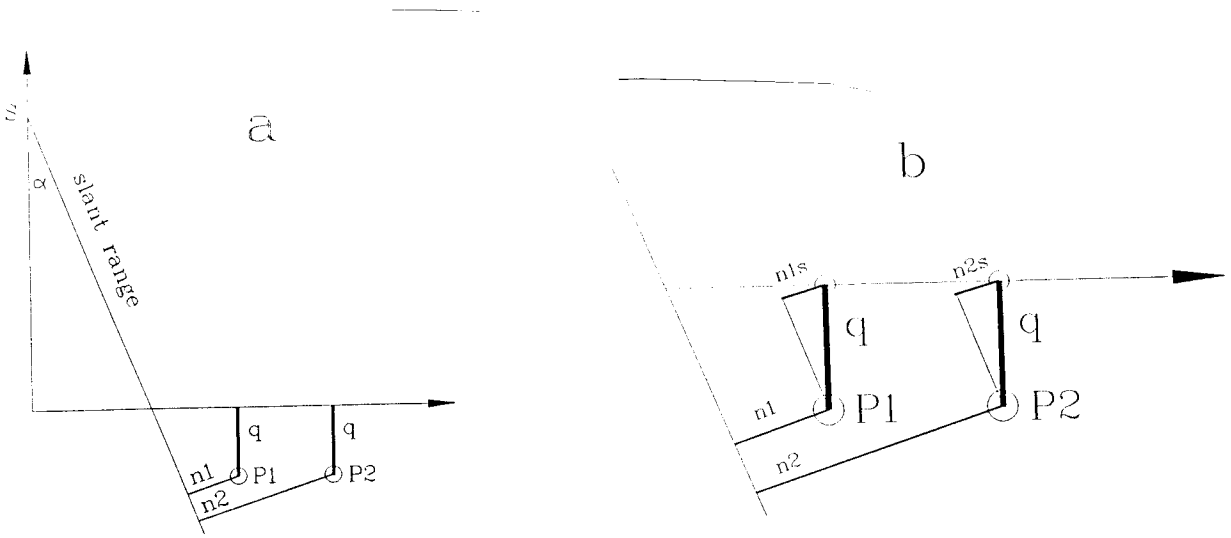

FIG. 5. Dependence of the normal displacement n_p on the terrain drop q before (a), and after (b) flat terrain compensation.

$$exp(\frac{-j2\omega_0}{ch\tan\alpha}n_s r) \quad . \tag{13}$$

After this conversion, the phase of $F_3(P)$ relative to a perfectly flat terrain, will be a constant. The expression of the phase difference $\Delta\psi$ thus becomes:

$$\Delta\psi = \frac{2\omega_0 n_s \Delta r}{ch}[\frac{1}{\tan(\alpha-\theta)} - \frac{1}{\tan\alpha}] \quad . \tag{14}$$

Examining Figure 5b, it is easy to see that after the subtraction of the normal displacement relative to the flat terrain, the normal displacement n_p of a point scatterer is proportional to the terrain drop q ($n_{1s} = n_{2s} = q/\sin\alpha$). The following expression of the phase difference then holds:

$$\Delta\psi = \frac{2\omega_0}{ch\sin\alpha}n_s q \quad . \tag{15}$$

Correspondingly, a phase wrapping period of the phase image corresponds to a terrain drop of

$$q = \frac{\pi c h \sin\alpha}{\omega_0 n_s} \quad . \tag{16}$$

EFFECTS OF THE FINITE RANGE RESOLUTION

So far, the system geometry of multiple SAR surveys has been described. In this section, we shall analyze the effects of the finite slant range resolution ρ (approx. 7 m for the SEASAT SAR; Rocca, 1987) on the system geometrical parameters. In the previous section, expressions of the phase difference $\Delta\psi$ were derived assuming, that the backscattered field measured by the satellite S_1 was coherent with that measured by S_2. The two measured fields, however, would be coherent everywhere (isotropic emission from the scatterer), only if the elementary scatterers were really point scatterers.

In practice, this is not the case, since the elementary cell is in fact characterized by a finite extension dependent on the range resolution. This cell acts as an antenna with a finite width and therefore the coherence between the two images is got only if the two satellites are within the the beam of the antenna corresponding to the cell, that is within an angle β proportional to the slant range resolution ρ. Further, the ground resolution ρ_g, or distance between the closest distinguishable points, also depends upon the terrain slope θ and the off-nadir angle α as (Rocca, 1987)

$$\rho_g = \frac{\rho}{\sin(\alpha - \theta)}. \tag{17}$$

The ground resolution ρ_g can be then regarded as providing the width of an equivalent antenna with an aperture angle

$$\beta = \frac{\lambda}{\rho_g}$$

(λ is the transmitted wave length). This antenna generates a "celestial footprint" at the satellite's distance h, whose linear aperture is βh.

In the case of SEASAT SAR images the "celestial footprint" angular aperture for a flat terrain is about 4.5 degrees, and its linear aperture is about 10 Km. For the flat terrain in this example, the normal displacement of the two satellites n_s must then be smaller than 10 Km. In the case of a dipping earth surface, the ground antenna width increases, and the celestial footprint shrinks.

EXPERIMENTAL RESULTS

The complex image $F_3(P)$ has been synthesized from SAR images of the Death Valley taken during three successive passes of the SEASAT SAR satellite (Li and Goldstein, 1987). Even if the satellite orbits were almost parallel, the focused

complex images had to be accurately aligned to maximize the signal-to-noise ratio of the phase image. The effects of incorrect alignment and image defocusing will be discussed later.

The normal displacement n_s between orbits has been computed by exploiting equation (11) and through measuring, on the phase images, the repetition period ΔR of the flat terrain area in the upper part of Figure 6. Figures 7 and 8 show, respectively, two interference fringe images of the same area shown in Figure 6. Figure 7-8 images were obtained by different survey combinations: the satellite orbits used for the first image are much closer - $n_s = 105$ m - than the other two - $n_s = 1250$ m .

The effect of the different orbit distances, n_s, is clearly visible on the two images. The repetition period ΔR of the first one is much greater than that of the second image.

Exploiting the equations found previously, we can identify the terrain slope limits that can be measured on the two images. In the case of the closer orbits, Figure 7, the greatest positive slope is about 19.3 degrees. In Figure 8 it is about 17.5 degrees. The phase of the modified images, obtained by zeroing the phase difference $\Delta\psi$ relative to the flat terrain, is shown in Figures 9 and 10 respectively. Taking advantage of equation (12), the terrain drop relative to a period ΔR can be computed: for the first image it is approximately 350 m; for the second one it is about 30 m.

The effect of an incorrect alignment of the two images used for the interference fringes generation of Figure 10, is shown in Figure 11. In Figure 11 the interference fringes image, obtained with one pixel range displacement ($\approx$ 20m), is shown. Figure 12, by contrast, shows the effect on the same image, of an incorrect focusing. An error of about two parts over 1000 on the satellite velocity has been introduced.

CONCLUSIONS

In this paper it has been shown that by exploiting multiple passes of a SAR system, terrain elevation can be measured. This technique can be usefully applied to define the nonlinear transformation necessary to avoid the well-known foreshortening effect clearly visible on hilly areas.

The interference fringe images presented in this paper show that the signal-to-noise ratio can be considered high enough.

Finally, it can be pointed out that the same analysis can be applied to tethered satellite SAR (Vetrella et al. 1987) systems avoiding the effects of time changes in the observed areas.

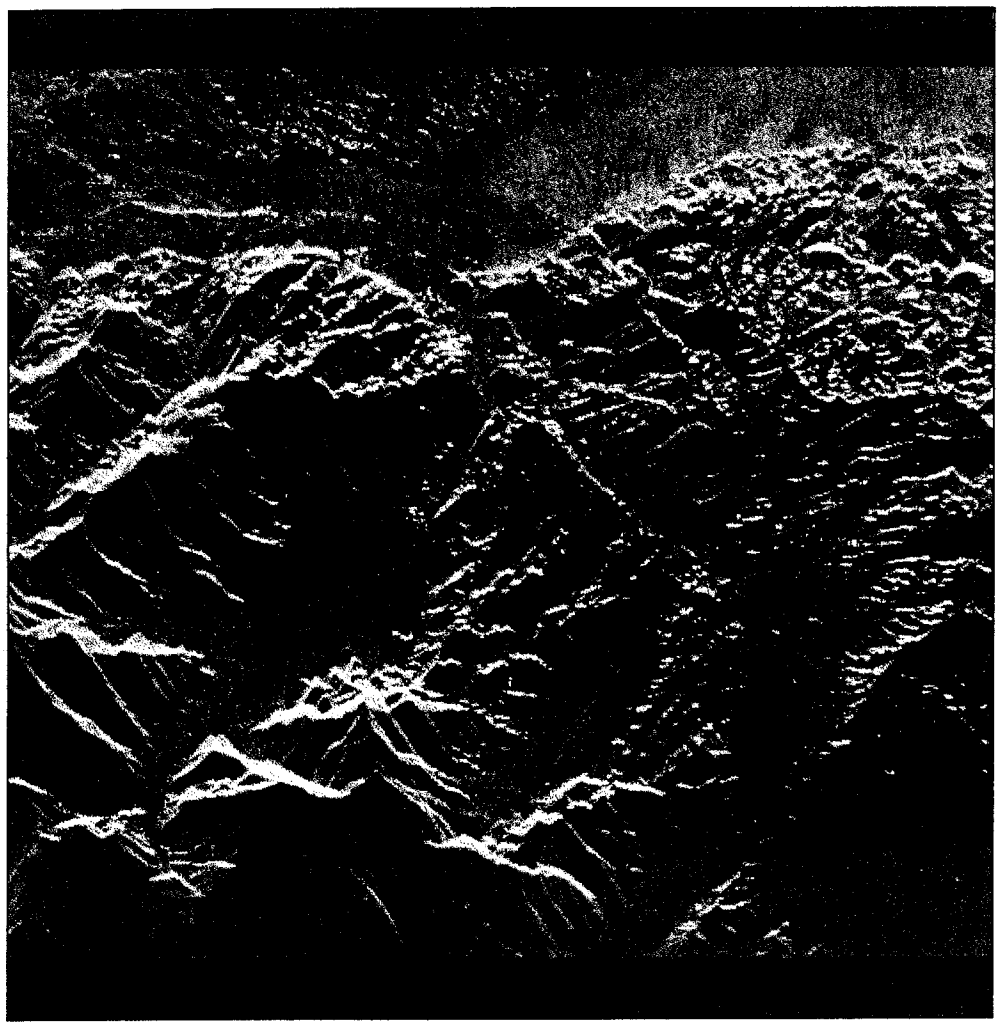

FIG. 6. SEASAT SAR image of the Death Valley area (approx. 20 x 20 Km)

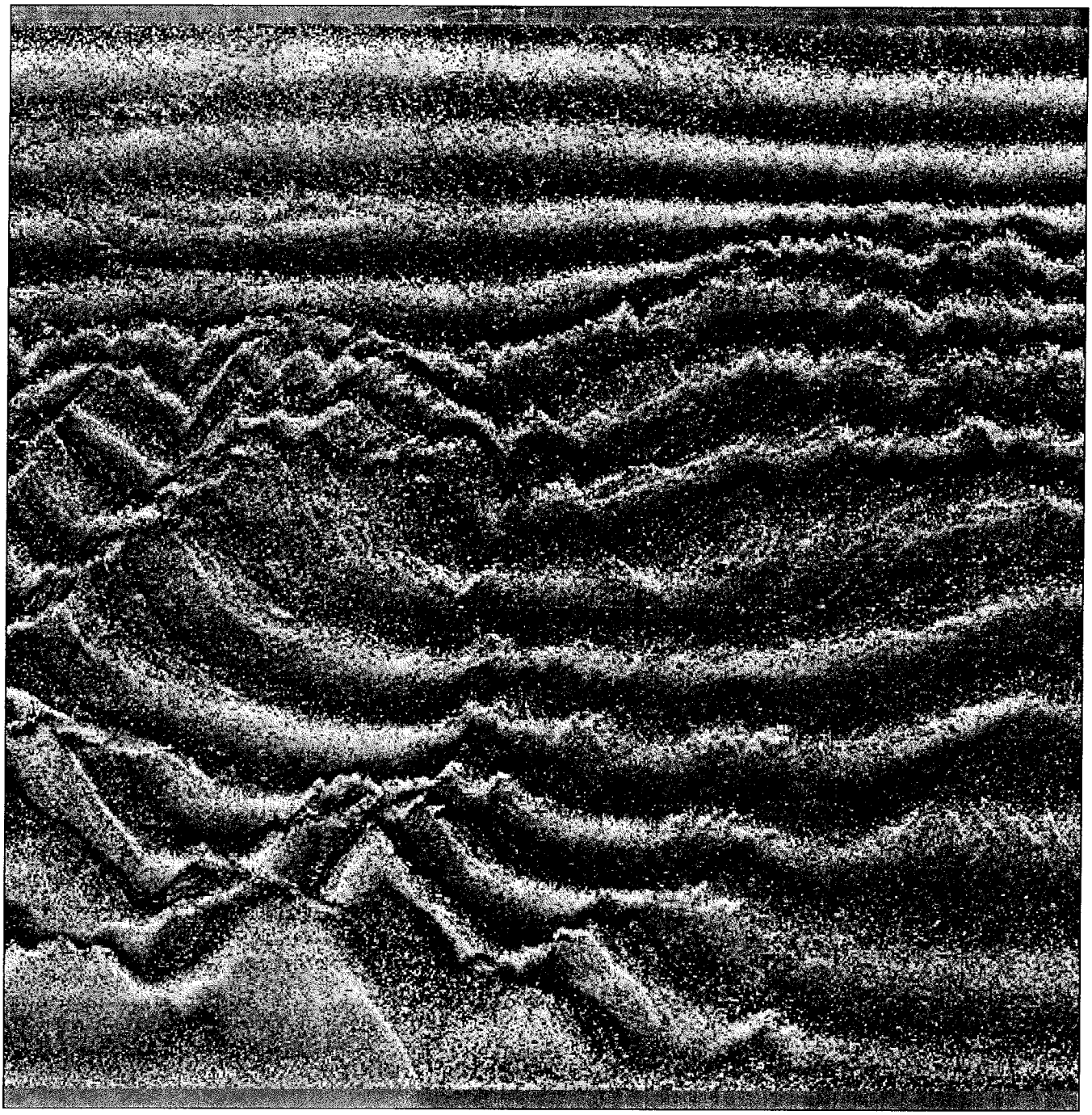

FIG. 7. Interference fringes of the SEASAT SAR image in Figure 6 . Ground resolution = approx. 40 x 40 m; orbits normal displacement = n_s = 105 m

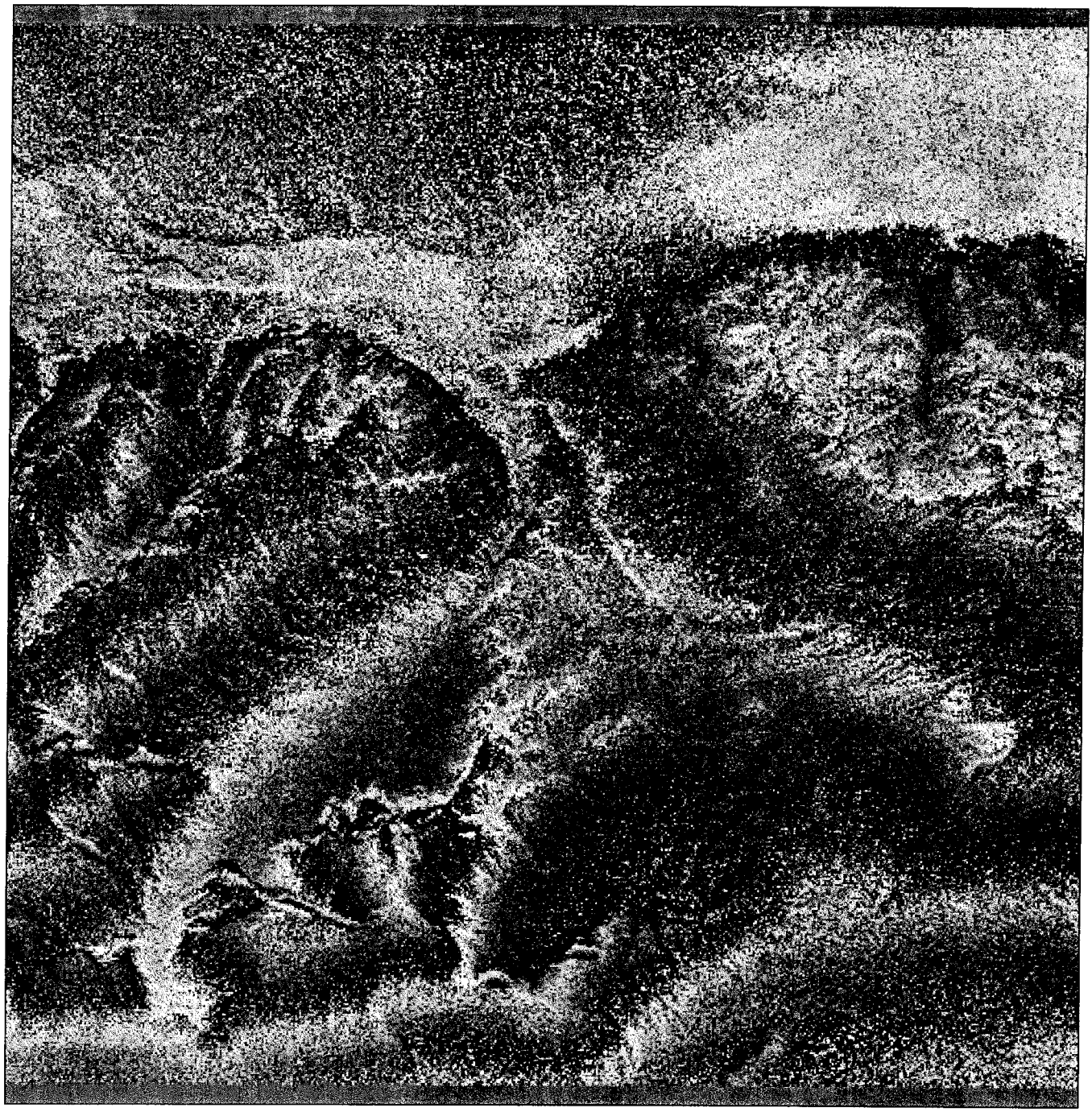

FIG. 8. The interference fringes shown in Figure 7 after flat terrain compensation. Ground resolution = approx. 40 x 40 m; orbits normal displacement is n_s = 105 m

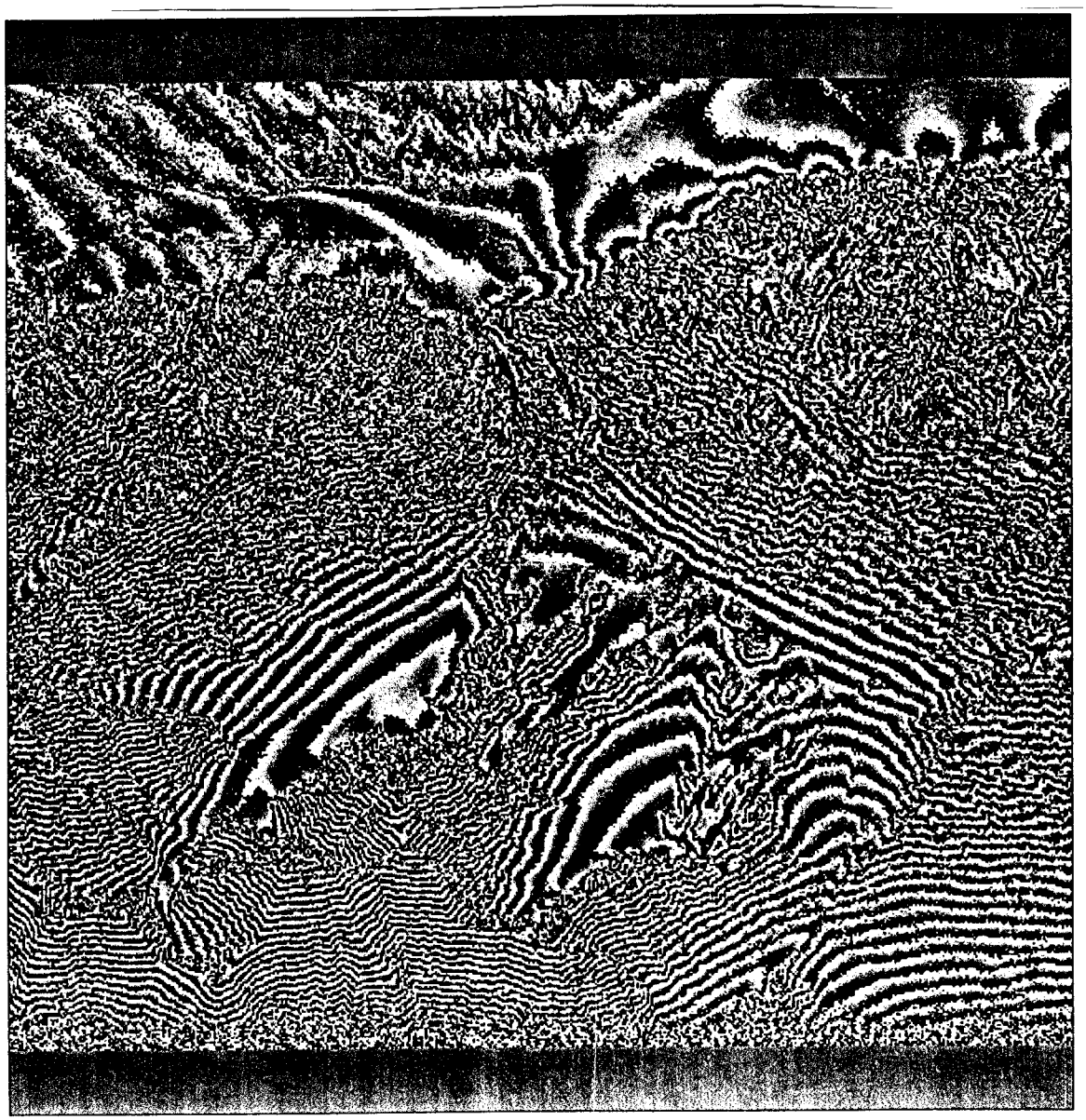

FIG. 9. Interference fringes after flat terrain compensation; ground resolution = approx. 40 x 40 m; the orbits normal displacement is now n_s = 1250 m. The alluvial fans in the valley (the semicircles in the upper part of the figure) are now quite visible.

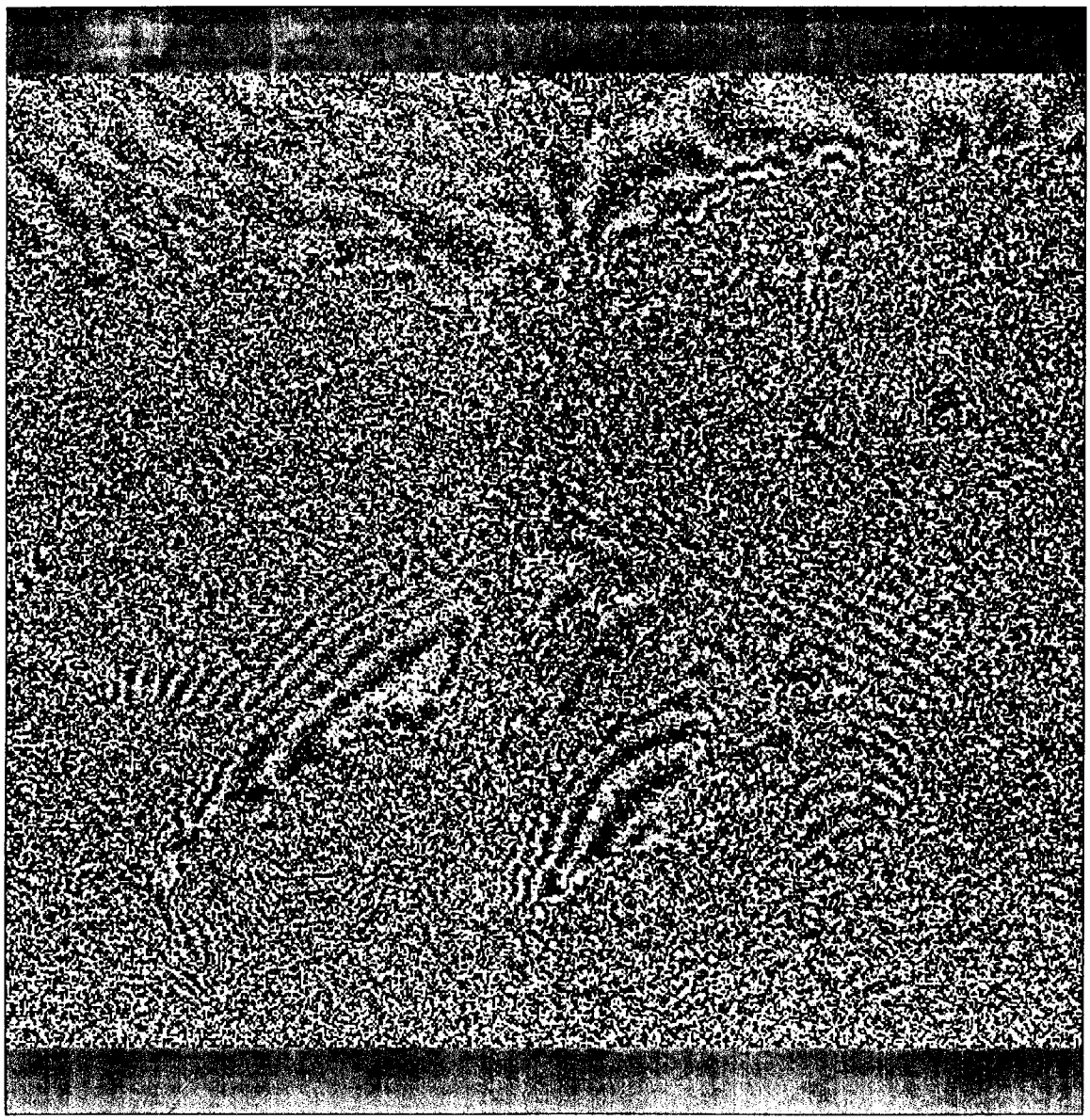

FIG. 10. The effect of one pixel range displacement upon the interference fringes of Figure 10.

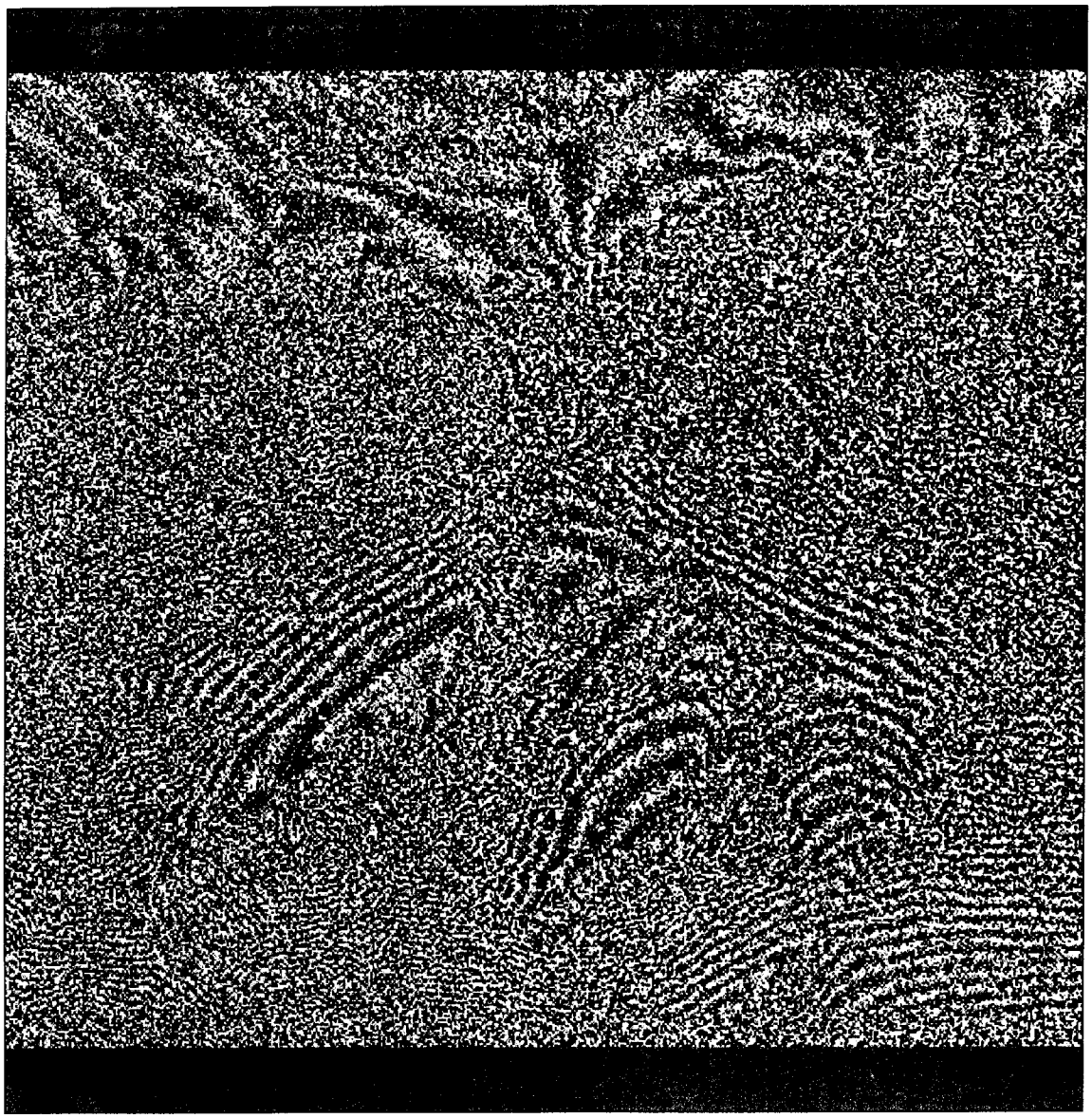

FIG. 11. Effect of two parts over 1000 satellite velocity error on the interference fringes of Figure 10.

ACKNOWLEDGMENT

The authors thank Drs. J. Curlander and R. Goldstein of JPL for the SEASAT SAR data. They express gratitude to the CSTS or Italian National Research Council for sponsoring one of the authors (C.P.) during the development of this work.

REFERENCES

Fitch, J. P., 1988, Synthetic Aperture Radar: Springer Verlag, New York 1988.

Li, F., and Goldstein, R., Studies of multibaseline spaceborne interferometric Synthetic Aperture Radar: Proc. of IGARSS '87 Symposium, Ann Arbor, May 1987, 1545 - 1549.

Ottolini, R., 1987, Synthetic aperture radar data processing: SEP – **56**, 203 - 214.

Rocca, F., 1987, Synthetic aperture radar: a new application for wave-equation techniques: SEP – **56**, 167-189.

Vetrella, S., Moccia, A., 1987, The tethered satellite system as a new remote sensing platform: Int. Journal on Remote Sensing, **8**, No.3, 309-323.

Zebker, H. A., Goldstein, R. M., 1985, Topographic mapping from interferometric Synthetic Aperture Radar observations: Proc. of the IGARSS '85, Amherst, Massachusetts.